ASEAN Engineering Journal

Full Paper

GROUNDWATER RESPONSE TO TIDES ON A SANDY BEACH

N.S. Rahim[a,b], Ilya K. Othman[a,b]*, M.H. Jamal[a,b], Z. Ismail[a,b]

[a]Faculty of Civil Engineering, Universiti Teknologi Malaysia (UTM), 81310 UTM Johor Bahru, Johor, Malaysia
[b]Centre for River and Coastal Engineering (CRCE), Research Institute for Sustainable Environment (RISE), Universiti Teknologi Malaysia (UTM), 81310 UTM Johor Bahru, Johor, Malaysia

Article history
Received
15 July 2023
Received in revised form
21 January 2024
Accepted
28 January 2024
Published online
31 August 2024

*Corresponding author
ilya@utm.my

Graphical abstract

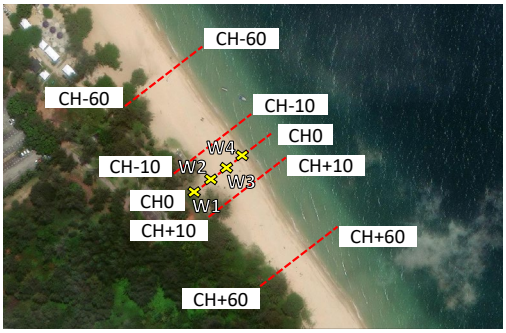

Abstract

Beach profile formation and morphology have been widely studied in recent years. A key point of understanding the dynamics of sandy beaches is the knowledge of the interactions between tides and groundwater with the beach profile, despite the challenges of conducting high-quality measurements. This study aims to clarify the response of groundwater levels to tides during two fieldworks: inter-monsoon (2017) and Southwest monsoon (2018) at Desaru Beach. Four monitoring wells were installed perpendicular to the beach, alongside a tide gauge, a wave buoy, and an underwater current meter. The findings showed that the water table was generally not flat but fluctuated with time following the tidal pattern at a tangent. Lag times observed in all wells ranged from 3 hours 20 minutes to no lag times during the spring and from about 4 hours 40 minutes to no lag times during the neap. The groundwater closest to the sea indicated a shorter lag time at high tides than low tides during the inter-monsoon and Southwest monsoon. This study indicated that the beach groundwater filled up faster than it drained between rising and falling tides. The time lags of groundwater levels established in this study can be utilised in coastal flood forecasting for similar beach conditions.

Keywords: Sandy beach, water table, tidal, morphology, waves

Kajian mengenai pembentukan dan morfologi profil pantai dijalankan secara meluas sejak kebelakangan ini. Satu perkara penting dalam memahami dinamik pantai berpasir adalah pengetahuan tentang interaksi antara pasang surut dan air bumi terhadap profil pantai, meskipun terdapat kesukaran dalam melakukan pengukuran berkualiti tinggi. Kajian ini bertujuan untuk menjelaskan respons paras air bumi terhadap pasang surut semasa dua kerja lapangan dijalankan iaitu antara-musim (2017) dan musim barat daya (2018) di Pantai Desaru. Empat perigi pemantauan dipasang secara serenjang dengan pantai, bersama-sama dengan tolok pasang surut, boya gelombang dan meter arus. Hasil kajian menunjukkan aras air secara umumnya tidak rata tetapi berubah mengikut corak pasang surut dengan tangen. Masa lengah yang dicerap dalam semua perigi pemantauan berjulat antara 3 jam 20 minit hingga tiada masa lengah semasa pasang surut perbani dan dari 4 jam 40 minit hingga tiada masa lengah semasa pasang anak. Air bumi dalam perigi pemantauan yang paling hampir dengan laut menunjukkan masa lengah yang lebih pendek semasa pasang tinggi berbanding pasang surut semasa antara-musim dan musim barat daya. Kajian ini menunjukkan bahawa air bumi memenuhi dengan lebih cepat daripada mengalir keluar antara pasang naik dan pasang surut. Masa lengah paras air bumi yang ditetapkan dalam kajian ini boleh digunakan dalam meramal banjir pantai untuk keadaan pantai yang serupa.

Kata kunci: Pantai berpasir, aras air, pasang surut, morfologi, gelombang

1.0 INTRODUCTION

The coastal zone occurs at the interface of three major natural systems on the Earth's surface: the atmosphere, ocean, and land surface [1]. The dynamics of the coastal zone are influenced by processes involving these systems. The coastal zone is important for various activities including transportation, agriculture, navigation, fisheries, aquaculture, and recreation. These activities promote economic growth in the country, making the sustainability of the coastal zone crucial to their success. In addition to the diverse coastal ecosystems and economic activities, the coastal zone also encompasses a significant groundwater system.

Groundwater naturally occurs in underground cracks, soil, sand, and rock spaces. It is defined as an equilibrium surface at which pore water pressure is equivalent to atmospheric pressure [2]. Groundwater occurs almost everywhere beneath the Earth's surface. The beach groundwater system is highly dynamic and can be simplified as a continuation of Mean Water Surface (MWS) from the sea, as seawater infiltrates and exfiltrates the beach. [3] has proposed an analytical solution for beach groundwater under the negligible influence of waves. The present study presents data with non-negligible waves. The shoreline is defined as the position where the MWS intersects, or simply the line of zero water depth [2] [3]. Groundwater on beaches is primarily affected by hydrodynamic factors such as tides, rainfall, waves, and sediment properties which influence hydraulic conductivity. Previous studies have shown that the water table is typically not flat, leading to a decoupling process between tides and groundwater levels.

[4] found that the decoupling occurs between tides and groundwater levels mainly due to the rapid drop of tides compared to the falling groundwater; see Figure 1(a). The groundwater level is higher than the tidal level during this process. Usually, this decoupling process occurs during the low tide at a flat beach and/or large tidal range [5]. When the tide rises, the tidal and groundwater levels are eventually coupled again, after which the groundwater level rises with the tide (Figure 1(b)) [6]. In short, the coupling and decoupling occur mainly influenced by the tides [7]. The groundwater exit point is a splitting position from the shoreline where the groundwater starts to outcrop or exfiltrate from the aquifer during falling tide. The decoupling process can be recognised easily from the formation of the seepage face or glassy surface along the shoreline. [8] stated that the formation of the seepage face occurs when run-up is faster than the exfiltration rate during the decoupling process. The intertidal zone, hydraulics properties, and the beach face's geometry influence the seepage face's boundary. Therefore, the degree of symmetry in the groundwater fluctuations will vary between beaches.

[9] highlighted that the position of the groundwater table in a beach aquifer is essential in shaping the beach profile. Earlier studies by [9] [10] [11] indicated that when the groundwater is higher than the Mean Sea Level (MSL), the beach sediment becomes liquefied and is likely to be eroded. Contrarily, if the groundwater is lower than the MSL, sediment siltation can cause accretion to occur. Several clarifications have been considered to describe this situation. One of them is the infiltration and exfiltration processes. When the groundwater level is low, the seawater will infiltrate rapidly into the beach above the water table until it reaches the hydrostatic equilibrium. This infiltration reduces the flow depth and velocity of the swash, thereby depositing the sediment to the beach. The beach is saturated when the beach face is wet and occurs mainly when the groundwater level exceeds the tidal elevation. Meanwhile, the formation of seepage face during ebb tides causes the decoupling process that increases the depth and velocity of backwash, thereby enhancing offshore transport. The groundwater outcropping to the surface can cause dilation or fluidisation of the sediment and will be carried away easily by the upcoming swash flows [9] [11].

The beach groundwater closer to the shoreline fluctuates with waves and tidal action in the swash zone. These forcings induce the cross-shore and longshore movement of sediment as the wave's energy ceases. Previous studies have highlighted the importance of interactions between the beach water table and tides on erosion and accretion processes above MSL [2] [12]. Studies involving tides, groundwater, and beach profile response ranged from eight weeks [13], six weeks [6] to four weeks [14]. [6] monitored sea surface elevation, groundwater in eight dip wells, surface moisture content, and wave, but they could not relate the relationship with rainfall or precipitation. [13] found that the infiltration into the intertidal saline cell is mainly controlled by high tides and freshwater exfiltration is due to the low tides. In contrast, deep saline exfiltration from below the freshwater exfiltration is negatively correlated to the low tides. However, the relationship between groundwater salinity the beach characteristics like slope and sediment sorting is unclear [13]. [14] installed 18 pressure sensors to examine those devices' ability to determine groundwater responses to tidal forcings. Their study showed that tides and wave climate affect most landward measurement points less. However, this study required a large amount of available data to process to identify the groundwater responses during tidal cycles with different wave forcing conditions. This paper better explains the dynamic interaction between groundwater, tides, and beach morphology on a sandy beach with a steep intertidal slope (approximately 1:7) at Desaru Beach. This knowledge is crucial for coastal management, protection against erosion, and planning sustainable coastal development.

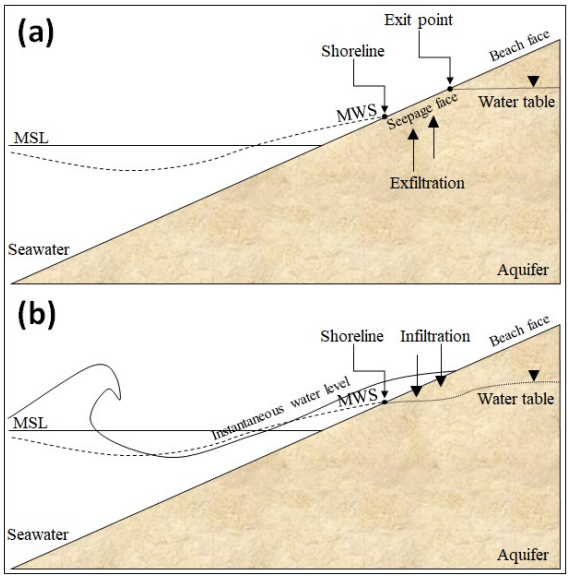

Figure 1 Schematic diagram of beach processes. (a) decoupling and (b) coupling (after [2])

2.0 METHODOLOGY

2.1 Field Site

The chosen site of Desaru on the East Coast of Johor Bahru is considered to be the most appropriate. Desaru consists of a 25 km white sandy beach and offers various activities parallel to the new tourism developments, making it a well-known beach in Johor. The site is located at a public beach in Desaru, situated between latitudes 1°30'N-1°38'N and longitudes 104°16'E-104°14'E. The South China Sea lies to the East while the Strait of Singapore to the South of Desaru. The beach area was bounded by two headlands: Tg. Balau in the North and Tg. Penawar in the South.

This beach has a medium sand particle classification, with sediment distribution, D_{50} ranging from 0.33 mm to 0.35 mm with an average porosity of 0.43 and an average density of 2635 kg/m^3 [15]. Desaru experiences two high tides and two low tides at unequal heights in one day, indicating a mixed semidiurnal tidal cycle [16]. The climate of the site area is equatorial monsoon. Desaru experiences four monsoons annually: the Northeast monsoon, or wet season, from November to March; the Southwest monsoon, or dry season, from May to September, and two inter-monsoon periods in April and October. According to [17], the annual mean temperature increases at Desaru, ranging from 0.3 to 0.4°C per decade from the average temperature of 27°C.

2.2 Data Collection

Two extensive fieldworks were carried out from the 6th to 13th of April 2017: for a full tidal cycle (neap to spring) during inter-monsoon and the 12th to 22nd of July 2018 for spring to neap during the Southwest monsoon at Desaru Beach. The topography survey was conducted from W1 (at x = 0) and up to x = 90 m for both fieldworks. Groundwater levels were determined using four monitoring wells: W1, W2, W3, and W4, in a cross-shore array at the site (Figure 2). These wells were constructed using a helical auger consisting of 0.05 m diameter PVC pipe with various pipe lengths according to the well location, ranging from 1.7 m (W4) to 5 m (W1). The more landward well usually requires a longer pipe length to reach the groundwater. The well locations were chosen based on the cross-shore profile, human activities, level of groundwater reach, and exposure to waves and currents. The previous failure occurred with a well installed approximately 30 m landward from W1, which became filled with water on the second day of installation during the 2017 fieldwork. The seaward well installed at 6.82 m from W4 also collapsed on the second day of installation during 2017 fieldwork due to wave impact and current circulation, causing instability to the pipe.

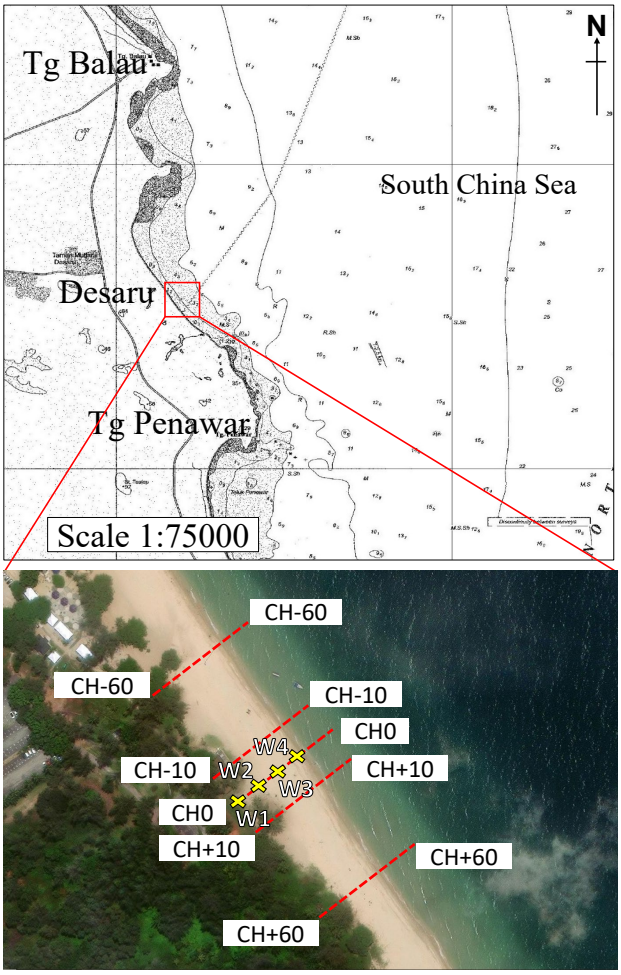

Figure 2 Location of Desaru Beach, Johor

Table 1 displays the latitude and longitude coordinates of the monitoring wells using World Geodetic System (WGS84) projections. The locations of these wells remain about the same for both fieldworks, except for W4, which was higher than MHHW in 2017 and located between MHHW and MSL in 2018 fieldworks. Figure 3 shows the general beach profile, wells' positioning, and sediment sampling points. Sediment samples were collected from a single cross-shore location, CH0. These sampling points, located at intervals of 20 to 35 meters, were strategically chosen to align with significant changes in Desaru beach morphology, specifically the upper swash, middle swash, and lower swash.

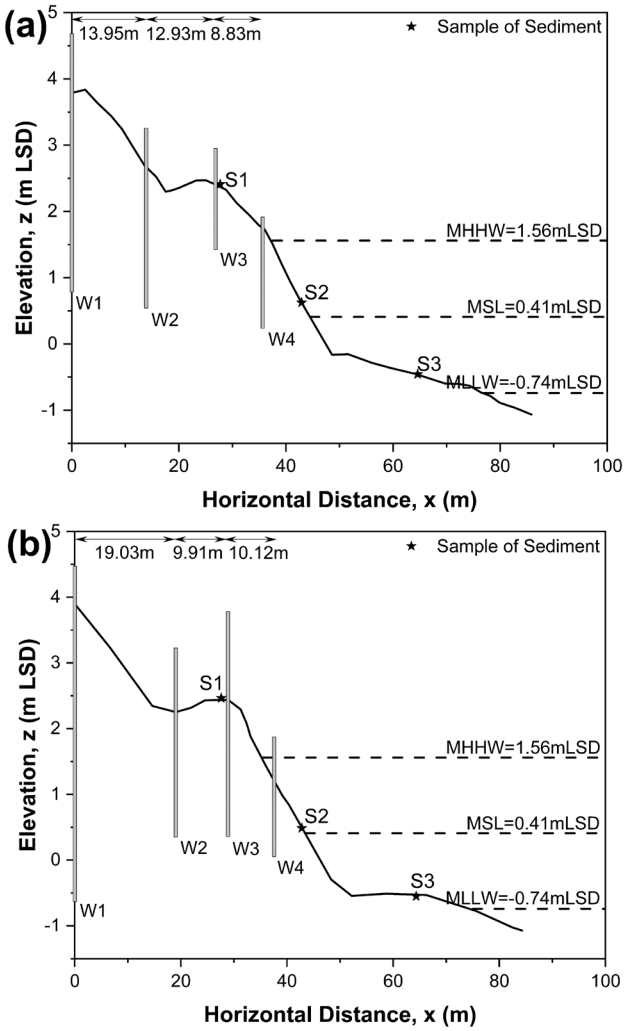

Figure 3 Positions of well and sediment sampling, (a) 6th – 13th April 2017 (neap to spring) and (b) 12th – 22nd July 2018 (spring to neap). The horizontal axis origin corresponds to W1

Table 1 Coordinates of monitoring wells at Desaru Beach

Well	2017		2018	
	Latitude (North)	Longitude (East)	Latitude (North)	Longitude (East)
W1	1° 32′ 43.83″	104° 15′ 56.98″	1° 32′ 43.84″	104° 15′ 57.01″
W2	1° 32′ 44.09″	104° 15′ 57.34″	1° 32′ 44.22″	104° 15′ 57.50″
W3	1° 32′ 44.35″	104° 15′ 57.68″	1° 32′ 44.42″	104° 15′ 57.75″
W4	1° 32′ 44.52″	104° 15′ 57.91″	1° 32′ 44.58″	104° 15′ 57.98″

From the 6th to the 13th of April 2017 and the 12th to the 22nd of July 2018, groundwater levels were determined continuously every 5 minutes for all wells. The water level loggers or sensors used in the wells were a Cera-Diver (Van Essen, Netherlands), a CTD-Diver (Van Essen, Netherlands), and two RBR*solo*^{3}D (RBR Ltd., Canada). The Cera-Diver, CTD-Diver, and RBR*solo*^{3}D are commonly used for in situ measurements of water quality parameters. These instruments typically have approximately ±0.05% FS (Full Scale) accuracy for water level measurements. The high level of precision is crucial for ensuring reliable and accurate monitoring of groundwater levels, making these instruments well-suited for environmental and hydrological applications. The same sensors were used for both fieldworks. The sensors were lowered into each monitoring well with a determined cable length. They were protected by a porous filter element at the lower end of each monitoring well to prevent sediment from infiltrating and touching the sensors. The water level loggers measured pressure, temperature, conductivity, water head, sea pressure, and depth for long and short-term recordings.

The elevation measurements include daily topographic surveys conducted at every low tide using standard levelling techniques, as well as Real-Time Kinematic (RTK) technology with the Topcon HiPer II (Topcon Corporation, Japan), along with Differential Global Positioning System (DGPS) for improved accuracy [18]. The DGPS comprises RTK stations and two receivers [19]. One receiver functions as a stationary ground-based reference station, transmitting the difference between the positions indicated by the satellite system and the known benchmark. The other receiver is a rover that moves around, measuring position distances from the base. All coordinates and heights determined during the fieldwork were measured in the Malayan Rectified Skew Orthomorphic (MRSO) coordinate system. The relatively broad intertidal region (around 100 m) allowed measurements at low tide up to x = 90 m from W1. However, due to the timing of low tide during nightfall and limited access during daylight, all topographic surveys were completed once a day during the whole field study.

The topographic surveys were conducted on selected chosen days along five cross-shore transects or chainages (CH), which were positioned at intervals of 10 m and 60 m apart (longitudinally). The middle transect was located at CH0, aligning with the position of the monitoring wells, as shown in Figure 2. The five chainages were chosen as the monitoring locations for the short-term changes in the beach profiles. Data obtained from RTK-GPS were converted and plotted into x-z coordinates (beach profile) for each chainage. The area of the beach profile is separated into several segments approximately equal in width. Differences between beach profiles (accrete or erode) are calculated from the difference of the beach profile from the start date for each fieldwork (6th April 2017 and 12th July 2018) and each segment. The trapezoidal rule is used to estimate the area under a curve. These areas under the curve represent the changes in area and were calculated for the five chainages. Mainline or CH0 was chosen for further analysis because the monitoring wells are all located at CH0 and uninterrupted by tourists.

The nearshore tidal elevation was derived from an in-situ Tide Gauge (TG) (Level TROLL 500 Data Logger, In-Situ Inc., US) installed at Tg. Balau jetty, 8 km North of the beach. The Level TROLL 500 Data Logger, like the Cera-Diver, CTD-Diver and RBR*solo*^{3}D, also typically offers an accuracy of approximately ±0.05% FS for water level measurements. The average bed level at Tg. Balau jetty during the 2017 and 2018 fieldwork were -0.53 m LSD and -0.62 m LSD, respectively. Tides or water level fluctuation measurements were taken at 5-minute intervals during the study periods for both fieldwork. The ability to translate the pressure signal to the water level or tides depends on the height of the water level sensor above the bed and is measured as often as possible. This tide gauge can be assessed every day during low tide. An Acoustic Doppler Current Profiler (ADCP) (Aquadopp Profiler 1 MHz, Nortek, US) and Current Meter Propeller (CM) (Model 106 Current Meter, Valeport Ltd.,

UK) were mounted on the seabed at approximately 10 m water depth, 1.8 km Northeast of the beach. The Current Meter Propeller has a current speed accuracy of ±0.004m/s for speeds below 0.15m/s and ±1.5% of the reading for speeds above 0.15m/s. On the other hand, the Acoustic Doppler Current Profiler has a velocity accuracy of ±1% of the measured value ±0.5 cm/s. This ADCP was used to measure the wave characteristics such as wave height, direction, and period every 30 minutes, while CM was used to measure the velocity, direction, and pressure every 10 minutes.

Only four data sets on the 10th and 12th of April 2017 and the 14th and 21st of July 2018 were chosen for analysis as these four sets have clear and identified profile features. Rainfall data were retrieved from the nearest rainfall station, Johor Silica (1541139), provided by the Department of Irrigation and Drainage Malaysia (DID).

3.0 RESULTS AND ANALYSIS

3.1 Nearshore Condition

Six samples from CH0 at Desaru Beach were subjected to sediment size analysis, which involved dry sieve analysis, small pycnometer testing to determine the specific gravity for soils with particles finer than 2 mm, and a constant head permeability test to determine the coefficient of permeability [20], following the methods outlined in BS 1377: Part 2: 1990. Figure 4 shows grading curves based on the observation from sieve tests. Median sediment particle size, D_{50} at Desaru Beach ranged from 0.40 – 0.41 mm (medium to fine sand) in 2017 and 0.42 – 1.6 mm (fine gravel to medium sand) in 2018 fieldwork, with the size ranges of particles referring to the British system [21]. Silt and clay are absent. The sediment size in the cross-shore direction did not vary significantly during the inter-monsoon of 2017 fieldwork. However, the sediment size increased in the onshore direction during the Southwest monsoon of 2018 fieldwork. This change may be attributed to the increasing wave energy and action during the Southwest monsoon, as well as changes in longshore drift patterns, resulting in the accumulation of coarser sediments in the onshore area. However, these factors are not covered in this study.

Figure 5 shows soil gradation of uniformly coefficient (C_u) and coefficient of gradation (C_c) for each sample during the fieldwork. C_u for all samples falls below three, indicating uniform soil, see Figure 5(a). Meanwhile, Figure 5(b) shows that all coefficients of gradation lie between 0.5 and 2.0, indicating that all soils are well-graded. This indicates that the sediment samples collected during the fieldwork may have relatively consistent particle sizes and good overall grading, which can affect their properties and behaviour. The coefficient of permeability, k resulting from a constant head permeability test performed using the S3 sample (below MSL) ranging from 0.14 cm/s to 0.16 cm/s in 2017 and 0.08 cm/s to 0.1 cm/s in 2018 fieldwork. High k values in 2017 fieldwork indicate possibilities of better drainage and less saturated beach compared to lower k values in 2018 fieldwork that may react vice versa [22]. The average particle density observed during the fieldwork in 2017 was measured at 2566 kg/m^3, while in 2018, the average particle density showed an increase to 2746 kg/m^3, indicating a significant variation in the composition of the sediment particles between the two fieldworks. All soil samples met the specific gravity standard for sand [23].

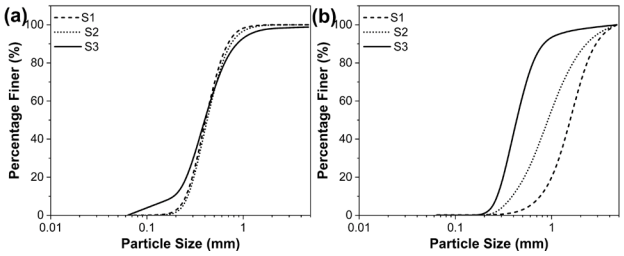

Figure 4 Particle-size distribution curve. (a) 12th April 2017 and (b) 19th July 2018

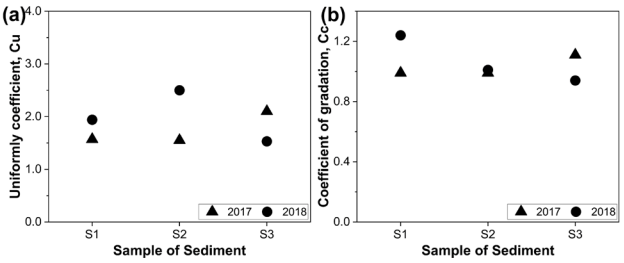

Figure 5 Soil gradation. (a) Uniformly coefficient and (b) coefficient of gradation

Figure 6 displays the nearshore tidal elevation (m LAT) observed at the TG Tg. Balau, measured using CM and from the nearest Tg. Sedili station, located 37.4 km North of Tg. Balau with coordinates 01°55'N and 104°07'E. The tidal elevation data from Tg. Sedili was derived through harmonic calculation, as documented in the annual Tide Table produced by the Royal Malaysia Navy. While the tidal elevation at TG Tg. Balau followed a similar pattern to that at Tg. Sedili, the frequency of the tides may differ due to the considerable distance between the two locations. Besides, the tidal elevation measured at TG Tg. Balau also followed a similar pattern with CM but at a lower frequency, especially during spring tide, as the CM is located approximately 6.85 km from TG Tg. Balau and located about 1.8 km offshore from the beach. The tide in the figure indicates two high tides and two low tides of unequal heights that occurred in a day, known as a mixed semidiurnal tidal cycle [24]. The tidal ranges in Figure 6(a) at Tg. Balau during neap and spring were 1.48 m and 1.72 m, respectively. Contrarily, the tidal ranges in the monsoon period for neap and spring at Tg. Balau were 1.23 m and 2.01 m (based on the last minimum reading) in Figure 6(b). The higher tidal difference in 2018 fieldwork occurred because of the missing water levels (tides) in Figure 6(b) which caused the tides to fall below the zero-tide gauge (0.65 m LAT or -0.62 m LSD). Hence, the tidal was expected to go lower than 0.65 m LAT or -0.62 m LSD, indicating dry conditions at Tg. Balau during that period.

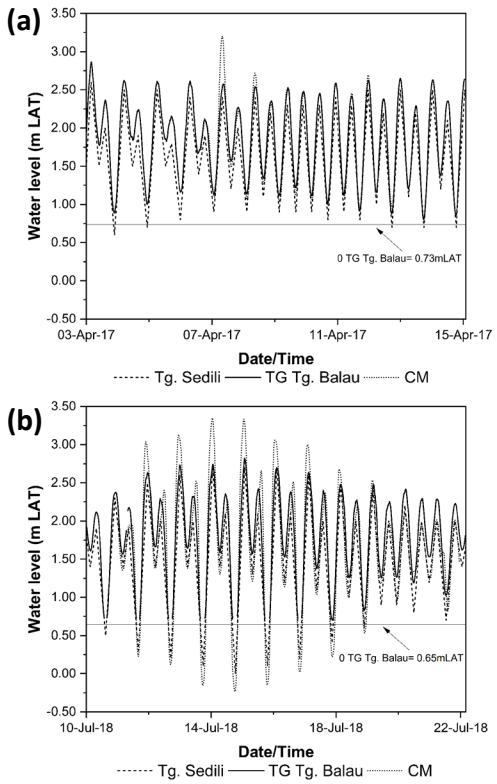

Figure 6 Nearshore elevation comparison at Tg. Sedili (Tide Table), TG Tg. Balau and CM. (a) 2017 fieldwork and (b) 2018 fieldwork

Figure 7 illustrates a closer investigation into tidal and groundwater fluctuations on (a) 10th April 2017 (neap), (b) 12th April 2017 representing spring (c) 14th July 2018 represents the spring and (d) 21st July 2018 represents the neap. However, during the 2017 fieldwork, there was a sensor malfunction in W2 and therefore, W2 data were not included in the analysis. The groundwater level time series from each well and the corresponding tides (Figure 7) were used to calculate lag times, as tabulated in Table 2. Examples of lag time determination for all wells and tides are given in Figure 7; points are marked in dotted circles. The groundwater levels in all wells, except W1 fluctuated in a pattern similar to the tides, though with varying lag times for each well. Lag times in W4 during 2017 fieldwork were longer compared to the 2018 fieldwork partly because it was located 2.11 m landward from the W4 in 2018 (see Figure 3).

The lag time designated an increasing trend with the increasing distance of the well from the shoreline (Table 2). As the lag time increased, the tidal forcing became insignificant to the groundwater response, and the water table fluctuations ceased [5] [25]. Due to its proximity to the shoreline, W4 showed a minimum lag time between groundwater levels at high tide and low tide during both the 2017 and 2018 fieldwork. Due to the missing water levels, the lag time determination at low tides for W2 and W3 was constrained in the 2017 fieldwork. W4 showed a slight difference between high and low tides for both spring and neap in 2018. The lag time differences at W4 were larger in 2017 than in 2018 because W4 was located further inland in 2018.

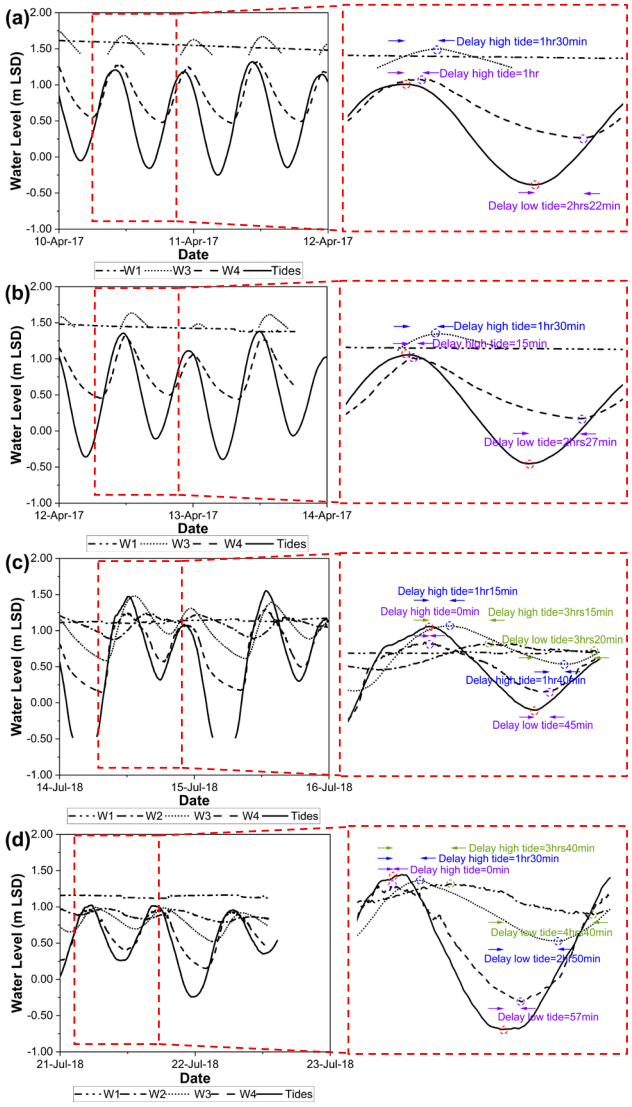

Figure 7 Groundwater level and tides. (a) 10th April 2017, (b) 12th April 2017, (c) 14th July 2018, and (d) 21st July 2018

Table 2 Lag time between tidal and groundwater

Well	10th April 2017		12th April 2017		14th July 2018		21st July 2018	
	Neap		Spring		Spring		Neap	
	High tide	Low tide	High tide	Low tide	High tide	Low tide	High tide	Low tide
W2	N/A	N/A	N/A	N/A	3 hrs 15 min	3 hrs 20 min	3 hrs 40 min	4 hrs 40 min
W3	1 hr 30 min	N/A	1 hr 30 min	N/A	1 hr 15 min	1 hr 40 min	1 hr 30 min	2 hr 50 min
W4	1 hr	2 hrs 22 min	15 min	2 hrs 27 min	0	45 min	0	57 min
Tidal range (m)	1.36		1.72		1.15		1.27	

Figure 8 shows the relationship between the daily mean groundwater level and daily inland rainfall at the nearest rainfall station, Johor Silica; located at 1°31'35"N and 104°11'05"E, approximately 9 km from the site. The classification of daily precipitation, as outlined by the World Meteorological Organisation (WMO) standard, is as follows: rain < 1 mm (no/tiny rain); 1 mm ≤ rain < 2 mm (light rain); 2 mm ≤ rain < 5 mm (low moderate rain); 5 mm ≤ rain < 10 mm (high moderate rain), 10 mm ≤ rain < 20 mm (low heavy rain); 20 mm ≤ rain < 50 mm (high heavy rain); and rain ≥ 50 mm (violent rain) [26]. During the period of study, the recorded rainfall either amounted to no rain or was less than the threshold for low heavy rain, with the exceptions occurring on 7th April 2017 (see Figure 8(a)) and 18th July 2018 (see Figure 8(b)). During the first fieldwork, there were 6 rainy days out of 8, with a total rainfall of 95 mm, while the second fieldwork experienced rain on 3 out of 11 days, totalling 36.5 mm of rainfall. The higher k values observed during the 2017 fieldwork, suggest the possibility of better drainage and a less saturated beach, which could contribute to the declining trend in the mean groundwater levels despite significant rainfall, see Figure 8(a). Conversely, the lower k values observed during the 2018 fieldwork, may indicate a beach with reduced drainage capacity and higher saturation, potentially contributing to the stable groundwater levels despite lower rainfall, see Figure 8(b). Overall, the correlation between inland rainfall and beach groundwater table was unclear. It is suggested that for future work, a rain gauge should be installed at the beach to provide a more accurate representation of rainfall and its impact on the beach groundwater response.

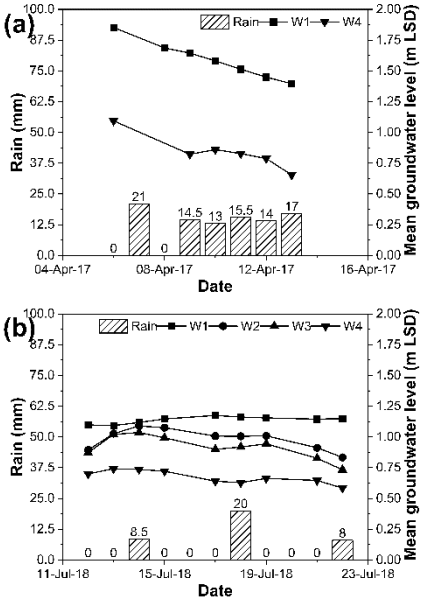

Figure 8 Daily mean groundwater level and daily rainfall. (a) 6th-13th April 2017 and (b) 12th-22nd July 2018

Figure 9 shows a wave rose analysis derived from the wave buoy data. Each colour's length represents the percentage frequency of waves coming from a specific direction, determined using the meteorological coordinate system (where North is 0 or 360 degrees and East is 90 degrees). The wave rose is split into five ranges based on different wave heights. In Figure 9(a), during the inter-monsoon period, 44.58% of waves with heights ranging from 0.2 to 0.8 m predominantly came from the East, while 33.25% and 2.36% originated from the Northeast and Southeast directions, respectively. The frequency of calm conditions, characterised by wave heights less than 0.2 m, accounted for approximately 19.81% of the observations.

In contrast, Figure 9(b) illustrates that the highest frequency of waves predominantly originated from the Southeast, with maximum wave height reaching 1.0 - 1.2 m and no waves below 0.2 m, resulting in a calm frequency of 0%. Table 3 presents the average wave and current data for the selected days. Overall, the average wave height during the spring and neap tides in 2018 was two to three times larger than in 2017 (Table 3). Based on the predominant wave direction, it is anticipated that cross-shore and longshore sediment transport will dominate the area in 2017 and 2018 respectively.

Figure 10 displays the time series of current velocity provided by CM during the fieldwork. The maximum current velocity during fieldwork in 2017 was 0.54 m/s, while in 2018, it reached 0.69 m/s. The average velocity was approximately the same for both fieldworks, at about 0.21 m/s. The highest current occurred on 15th July 2018 around 02:00 A.M., with a velocity of 0.69 m/s before reducing its magnitude following the neap tidal cycle.

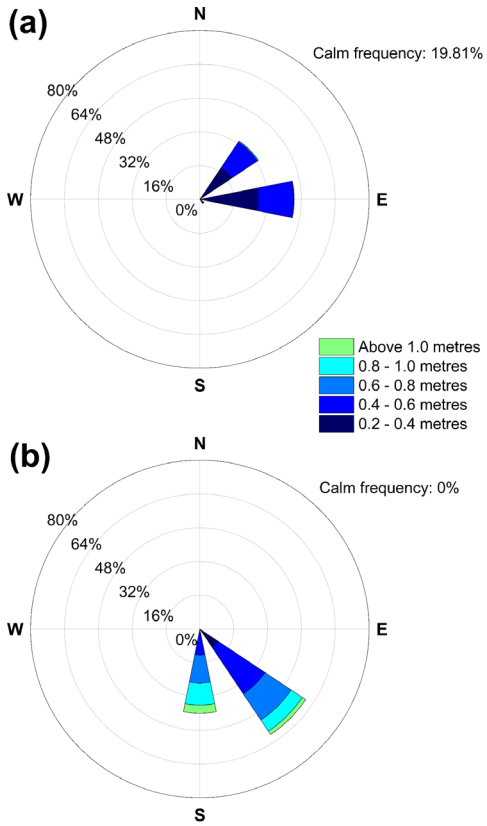

Figure 9 Wave rose. (a) 6th – 13th April 2017 and (b) 12th – 22nd July 2018

Table 3 Average wave and current characteristics

	10th April 2017	12th April 2017	14th July 2018	21st July 2018
Wave height, Hm_0 (m)	0.21	0.18	0.71	0.45
Wave direction (°N)	66.93	92.51	157.15	153.56
Peak wave period, T_p (s)	6.12	5.04	4.98	4.36
Current velocity (m/s)	0.18	0.17	0.26	0.13

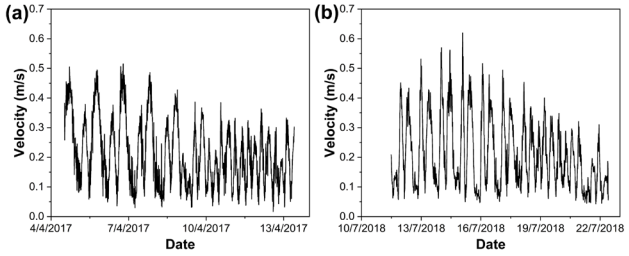

Figure 10 Velocity time series. (a) 6th – 13th April 2017 and (b) 12th – 22nd July 2018

3.2 Beach Profile

The overall cross-sectional area changes for five chainages are presented in Figure 11, with each chainage measured at approximately 60 m in length. Positive (+) and negative values (-) of area changes indicate deposition and erosion, respectively. The results indicated that CH60 on 21st July 2018 experienced the highest area changes, with a notable erosion of -9.08 m^2, as might be expected due to the increased human activity in this area. Near CH-60 during the 2018 fieldwork, ongoing development is taking place, leading to the occasional passage of a bulldozer through this chainage. Meanwhile, near CH60 in the same fieldwork, a drainage pipe was present, disturbing the normal bed profile. The area changes during the Southwest monsoon are categorised by the interchange of erosion and accretion, as observed in Figures 11(c) and 11(d). Overall, the net accretion process was dominant on the 10th and 12th of April 2017, while the beach was greatly eroded on the 14th and 21st of July 2018.

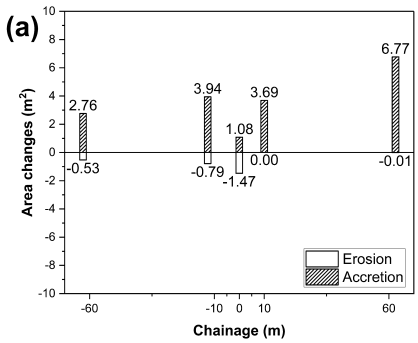

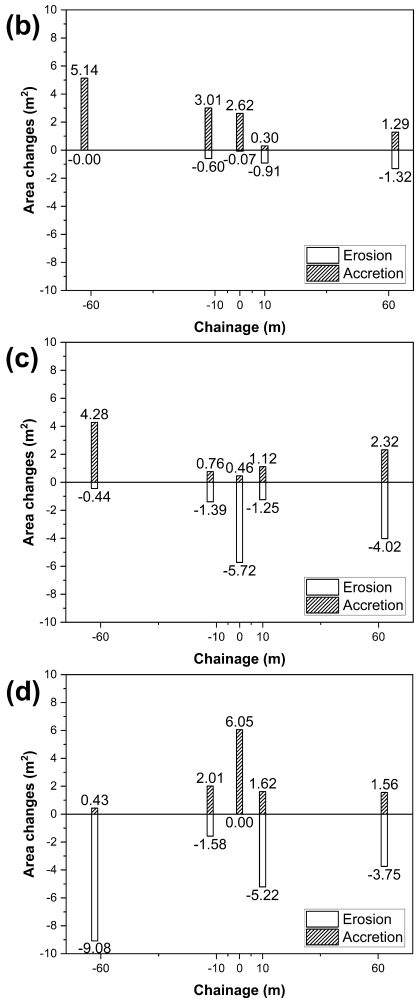

Figure 11 Cross-sectional area changes. (a) 10th April 2017, (b) 12th April 2017, (c) 14th July 2018, and (d) 21st July 2018. Accretion (diagonal stripes bar) and erosion (solid bar)

Figures 12 and 13 are plots of the tides and groundwater levels on the beach profile in 2017 and 2018, respectively. The following description simplifies the dynamic tidal fluctuation into four primary scenarios within the tidal cycle, beginning from the top to bottom figures representing (i) at half-rising tides, (ii) at high tides, (iii) at half-falling tides, and (iv) at low tides. The groundwater values in Figures 12 and 13 are taken simultaneously with tidal level data. It is important to note that due to sensor malfunction, W2 was eliminated, and W3 was only counted during high tide and half-falling tides in Figure 12.

The position of water tables in Figure 12 was always higher than tidal elevation during the inter-monsoon for neap and spring. Small changes in tidal ranges between neap and spring tides, combined with calm conditions and low current velocity predominantly from the East, contributed to the formation of a gentle, smooth, and wider beach face (from the crest of the berm to the step crest) with berm formation around x = 17 – 28 m. The changes in beach profile over the neap-spring cycle are significant, transitioning from a 19 m width beach face and $\tan\beta$ = 0.13 slope (Figure 12a) to a 23 m width beach face and $\tan\beta$ = 0.11 slope (Figure 12b). The trend of groundwater and tidal movements towards hydrodynamic equilibrium was unclear due

to W4 being located around 0.69 m above MHHW, creating disconnections between groundwater and sea level.

During the Southwest monsoon (Figure 13), the groundwater and tides moved closer towards the hydrodynamic equilibrium stage at the land-sea boundary, except for Figure 13a(ii). Higher Southerly wave heights and large changes in tidal ranges have led to the formation of a well-developed berm around x = 16 – 30 m with a net berm cross-sectional area of 1.02 m^2 at a steeper seaward slope, $\tan\beta$ = 0.14 and a narrow beach face around 18 m wide (Figure 13a and Figure 13b). The beach profiles indicated a step crest underwater accretion at around x = 47 m during spring (Figure 13a) and slightly seaward around x = 49 m during neap (Figure 13b). The foreshore movement of the underwater step crest location during neap may be due to greater undertow currents in ebbing tides, causing the sediment to deposit farther. Figure 13a(ii) shows the tidal elevation was higher than the groundwater level by 0.24 m LSD, reflecting a possible saline intrusion (infiltration) in W4. However, if the seawater is constantly higher than the groundwater, not only does saline intrusion occur but land submergence will follow, usually as a consequence of rising sea levels or overexploitation of groundwater in a coastal aquifer [27] [28].

The transition from neap to spring in the 2017 fieldwork indicated a steeper hydraulic gradient than from spring to neap in 2018. There was a tendency for the seepage face to be larger during the 2017 fieldwork owing to the bigger difference between tides and groundwater than in the 2018 fieldwork most of the time. This suggested a longer time of decoupling between tides and groundwater. Comparatively, in the 2018 fieldwork, it was predicted that the seepage face would be smaller than in 2017 and tides would coincide with ocean tides most of the time, indicating a coupling between tides and groundwater. Further data collection and analysis are required to determine the influence of seepage face towards the decoupling process.

A larger hydraulic gradient was observed during half-rising tides in Figures 12a-b(i) and 13a-b(i), and low tides in Figures 12a-b(iv) and 13a-b(iv) in both fieldworks, indicating the possibility of higher discharge of groundwater (exfiltration) into the sea compared to high tide (Figure 12(ii) and 13(ii)) and half falling tide (Figure 12(iii) and 13(iii)). A large hydraulic gradient caused the groundwater to exfiltrate from the saturated beach face and decouple with tides [14]. The sloping beach face responds as a non-linear filter that influences the groundwater level to increase steeply and decrease gradually compared to the near-sinusoidal tides, which govern the forcing [5]. In general, the exfiltration process takes longer than the infiltration process and may not coincide precisely with rising and falling tides, depending on the distance of the beach groundwater to the shoreline [16] [29]. The infiltration and exfiltration rates can be attributed to accretion and erosion processes on Desaru Beach and are subjected to further analysis.

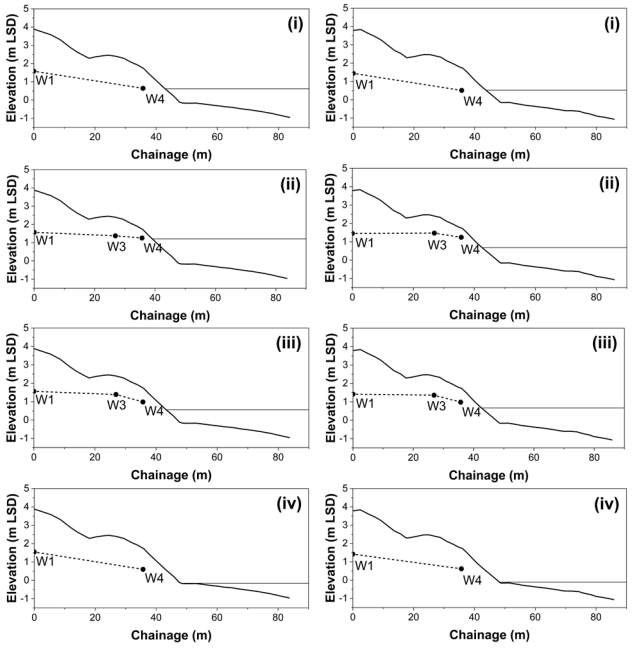

(a) 10th April 2017 (Neap) (b) 12th April 2017 (Spring)

Figure 12 Water table elevation (dashed line with dots from W1 at left to W4 at right), beach (solid line). From top to down. (i) half-rising tide, (ii) high tide, (iii) half falling tide, and (iv) low tide

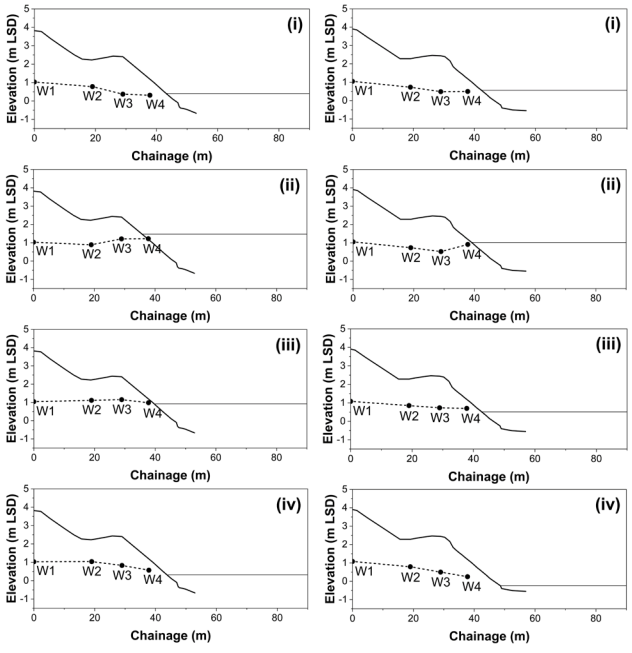

(a) 14th July 2018 (Spring) (b) 21st July 2018 (Neap)

Figure 13 Water table elevation (dashed line with dots from W1 at left to W4 at right), beach (solid line). From top to down. (i) half-rising tide, (ii) high tide, (iii) half falling tide, and (iv) low tide

The sediment sizes (D_{50}) between the berm and step crest ranged from 0.40 to 0.41 mm in 2017 fieldwork and 0.42 to 1.60 mm in 2018 fieldwork. The berm and step formation are categorised as independent features due to onshore swash

asymmetry during the spring-neap cycle. The step is formed due to sediment convergence at the wave breaking point and is linked to mixed semidiurnal tides [30]. Overall, the beach profile morphology in this study mostly changes between -0.50 to +2.5 m LSD. This finding was consistent with the findings of [31], who highlighted that the strongest variability of beach profiles at Desaru Beach occurred at the intertidal level boundary (between -0.74 and +2.0 m LSD).

4.0 CONCLUSION

Field measurements of cross-shore beach profile, beach groundwater, and tides were conducted for eight and eleven consecutive days during the 2017 and 2018 fieldwork, respectively. Desaru Beach is characterised as a fine gravel to fine sandy beach with a mixed semidiurnal tidal cycle. The missing tide data on 14th July 2018 affected the calculation of tidal ranges and lag time. Observations from all the monitoring wells indicated that the water table was generally not flat but fluctuated with time following the tidal pattern at a tangent. The lag times in all functioning wells except W1, ranged from 3 hours 20 minutes to no lag times during the spring and from about 4 hours 40 minutes to no lag times during the neap. The landward monitoring well, W1 was weakly affected by the tides. This study indicated that the beach groundwater filled up faster than it drained between rising and falling tides. The time lags of the groundwater level established in this study can be utilised in coastal flood forecasting for similar beach conditions. The correlation between beach groundwater levels and inland rainfall during this fieldwork was not visible due to the inland rainfall station being located 9 km from the study area. Results obtained from the wave rose indicated predominant Easterly waves in 2017 and Southeasterly waves in 2018, suggesting possible cross-shore and longshore sediment transport domination in 2017 and 2018, respectively. Water tables were expected to be disconnected to tidal level during the 2017 fieldwork (inter-monsoon) for neap and spring. The beach profile in 2017 (during inter-monsoon) fieldwork indicated a smooth and gentle shape with a weak form of a berm around x = 17 - 28 m and almost no net berm area changes. In 2018 during the Southwest monsoon, the beach profile indicated a well-developed berm around x = 16 - 30 m, with a net berm cross-sectional area of 1.02 m^2 on 21st July 2018. Additionally, beach profiles during the 2018 fieldwork showed a clear underwater step crest around x = 47 m (neap) and x = 49 m (spring) compared to the 2017 fieldwork.

Acknowledgement

The authors would like to acknowledge the financial support from the Ministry of Education Malaysia under Fundamental Research Grant Scheme (FRGS) (FRGS/1/2016/TK01/UTM/02/4) and Universiti Teknologi Malaysia for the funding under UTM Fundamental Research (UTMFR) (Q.J130000.3851.21H77). Many people and organisations have helped throughout this study. In particular, the authors would like to express appreciation to Desaru Coast for granting the site permission and for the assistance provided by the support staff and graduate students throughout the fieldwork.

References

[1] Davidson-Arnott, R. 2010. *An Introduction to Coastal Processes and Geomorphology.* United States, Cambridge University Press.
[2] Horn, D.P. 2002. Beach Groundwater Dynamics. *Geomorphology*, 48: 121-146. DOI: http://dx.doi.org/10.1016/S0169-555X(02)00178-2
[3] Nielsen, P. 1988. Wave setup: A Field Study. *Journal of Geophysical Research*, 93 (C12): 15643-15652
[4] Horn, D.P. 2006. Measurements and Modeling of Beach Groundwater Flow in the Swash Zone: A Review. *Continental Shelf Research*, 26: 622-652. DOI: http://dx.doi.org/10.1016/j.csr.2006.02.001
[5] Nielsen, P. 1990. Tidal Dynamics of the Water Table in Beaches. *Water Resources Research*, 26(9): 2127-2134
[6] Brakenhoff, L. 2015. Interaction of Tides, Groundwater Levels and Surface Moisture on a Sandy Beach. Master diss., Utrecht University, Netherlands
[7] Chen, W., Van Der Werf, J.J. and Hulscher, S.J.M.H. 2023. A Review of Practical Models of Sand Transport in the Swash Zone. *Earth-Science Reviews.* 238: 104355. DOI: http://dx.doi.org/10.1016/j.earscirev.2023.104355
[8] Cartwright, N. 2004. Groundwater Dynamics and the Salinity Structure in Sandy Beaches. PhD diss., University of Queensland, Australia
[9] Grant, U.S. 1948. Influence of the Water Table on Beach Aggradation and Degradation. *Journal of Marine Research*, 7: 655-60
[10] Turner, R.J. 1990. The Effects of a Mid-Foreshore Groundwater Effluent Zone on Tidal-Cycle Sediment Distribution in Puget Sound, Washington. *Journal of Coastal Research,* 6 (3): 597-610
[11] Baird, A.J., Horn, D.P., Mason, T.E. 1998. Validation of a Boussinesq Model of Beach Groundwater Behaviour. *Marine Geology* 148: 55– 69 DOI: http://dx.doi.org/10.1016/S0025-3227(98)00026-7
[12] Bakhtyar, R., Brovelli, A., Barry, D.A., Li, L. 2011. Wave-Induced Water Table Fluctuations, Sediment Transport and Beach Profile Change: Modeling and Comparison with Large-Scale Laboratory Experiments. *Coastal Engineering*, 58(1): 103-118. DOI: http://dx.doi.org/10.1016/j.coastaleng.2010.08.004
[13] Abarca, E., Karam, H., Hemond, H.F. and Harvey F. 2013. Transient Groundwater Dynamics in a Coastal Aquifer: The Effects of Tides, the Lunar Cycle and the Beach Profile. *Water Resources Research*, 49: 2473-2488. DOI: http://dx.doi.org/10.1002/wrcr.20075
[14] de Drézigué, O.D., Sous, D., Lambert, A., Gouaud, F. and Rey, V. 2009. Water table Response to Tidal Forcing in the Truc-Vert Sandy Beach. *Journal of Coastal Research*, SI 56: 1761-1765
[15] Berahim, M. 2014. Longshore Sediment Transport in the Swash Zone at Desaru Beach. Master diss., Universiti Teknologi Malaysia, Malaysia
[16] Rahim, N.S., Jamal, M.H., Abd Wahab, A.K., Othman, I.K., Ismail, Z., Othman, N. and Sa'ari, R. 2016. Sandy Beach Profile Evolution. *Malaysian Journal of Civil Engineering*, 28(3): 301-313. DOI: http://dx.doi.org/10.11113/mjce.v28n0.466
[17] The World Bank Group and the Asian Development Bank. 2021. Climate Risk Country Profile: Malaysia. World Bank Publications.
[18] Dłużewski, M. Dłużewska, J.R., Hesp, P.A., Tomczak, J.O. and Dubis, L. 2023. Impact of Coastline Orientation on the Dynamics of Foredune Growth. *Miscellanea Geographica* 27(4): 147-156 DOI: http://dx.doi.org/10.2478/mgrsd-2023-0020
[19] Łabuz, T.A. 2016. A Review of Field Methods to Survey Coastal Dunes-Experience Based on Research from South Baltic Coast. *Journal of Coastal Conservation*, 20(20): 175-190. DOI: http://dx.doi.org/10.2478/mgrsd-2023-0020
[20] Head, K.H. 2006. *Manual of Soil Laboratory Testing*- Soil Classification and Compaction Tests. 1. Whittles Publishing, UK
[21] British Standard Institution 1990. British Standard Methods of Test for Soils for Civil Engineering Purpose, Part 2: Classification Test. London: BS1377
[22] Saponieri, A. and Damiani, L. 2015. Numerical Analysis of Infiltration in a Drained Beach. *International Journal of Sustainable Development and Planning*. 10: 467-486 DOI: http://dx.doi.org/10.2495/SDP-V10-N4-467-486
[23] Das, B.M. 2011. Principles of Foundation Engineering, SI Seventh Edition. Cengage Learning, USA
[24] Reeve, D., Chadwick, A. and Fleming, C. 2012. Coastal Engineering: Processes, Theory and Design Practice. USA and Canada, Spon Press
[25] Hegge, B.J. and Masselink, G. 1991. Groundwater-table Responds to Wave Run-up: an Experimental Study from Western Australia. *Journal of Coastal Research,* 7 (3): 623-634

[26] Tan, M.L., Ibrahim, A.L., Duan, Z., Cracknell, A.P. and Chaplot, V. 2015. Evaluation of Six-High Resolution Satellite and Ground-Based Precipitation Products over Malaysia. *Remote Sens.*, 7: 1504-1528 DOI: http://dx.doi.org/10.3390/rs70201504

[27] Urish, D.W. and McKenna, T.E. 2004. Tidal Effects on Groundwater Discharge through a Sandy Marine Beach. *Groundwater*, 42(7): 971-982

[28] Alfarrah, N. and Walraevens, K. 2018. Groundwater overexploitation and seawater intrusion in coastal areas of arid and semi-arid regions. *Water*, 10(2): 143. DOI: http://dx.doi.org/10.3390/w10020143

[29] Othman, N., Abd Wahab, A.K. and Jamal, M.H. 2014. Effects of Seasonal Variations on Sandy Beach Groundwater Table and Swash Zone Sediment Transport. *Proceedings of 34th Conference on Coastal Engineering. Coastal Engineering Research, California,* 1-12. *ISBN 978-0-9896611-2-6.*DOI: http://dx.doi.org/10.9753/icce.v34.sediment.59

[30] Austin, M.J. and Buscombe, D. 2008. Morphological Change and Sediment Dynamics of the Beach Step on a Macrotidal Gravel Beach. International *Journal of Marine Geology*, Geochemistry and Geophysics. 249: 167-183. DOI: http://dx.doi.org/10.1016/j.margeo.2007.11.008

[31] Othman, N. 2019. Influence of Seasonal Hydrological Variation on Swash Zone Morphological Changes. PhD thesis, Universiti Teknologi Malaysia, Malaysia